INTERNATIONAL SOCIETY FOR SOIL MECHANICS AND GEOTECHNICAL ENGINEERING

Calibration and limitations of a fixed-partly fixed resonant column apparatus

Luke Rieman[1#], *Róisín* Buckley[1], and *Simon* Wheeler[1]

[1]*University of Glasgow, Jam School of Engineering, G12 8LT,* Glasgow, United Kingdom
[#]*Corresponding author: l.rieman.1@research.gla.ac.uk*

ABSTRACT

The small-strain shear modulus of soils and rocks is an important input parameter in geotechnical analyses. Its estimation using the resonant column apparatus relies on accurate knowledge of the rotational inertia of the apparatus's active end. Due to the complex geometry of the active end, its inertia is typically found from a calibration exercise. In this study a range of aluminium calibration bars and steel masses were used to compare two different calibration exercises presented in the literature. The resulting values of active end inertia are shown to be highly method-dependent. The method of compensating for the drive connection stiffness by finding the apparatus resonant frequency is found to introduce errors at low stiffness. The combined use of calibration bars and masses reduces scatter but yields poor results for stiff bars. An alternative approach to mitigate both of these problems is suggested. Active end inertia is found to be constant using this alternative approach. While effects of base inertia and reaction mass inertia are found to be small for this apparatus, compliance of the drive system is shown to significantly reduce resonant frequencies at high stiffnesses which increases the apparent active end inertia. This reduction in resonant frequency is modelled and used to derive frequency correction factors, which reduce errors in shear modulus to within acceptable limits when using the constant value of active end inertia. This demonstrates the potential for increasing the limit of sample stiffness where sufficient calibration data are available.

Keywords: Hardin resonant column; calibration; soil stiffness; apparatus limits.

1. Introduction

For many geotechnical analyses involving dynamic or cyclic loading the strain amplitudes generated in the soil are relatively low and therefore the small-strain shear modulus, G_0, and damping ratio, D_s, are key parameter inputs. Dynamic measurement techniques such as the resonant column approach or wave propagation via bender elements are often used to obtain the small strain stiffness in the laboratory. The resonant column test involves excitation of a cylindrical specimen in its fundamental mode of vibration to find the shear wave velocity, V_s, which can be used to calculate the small strain stiffness, G_0, using elastic theory:

$$G_0 = \rho V_s^2 \tag{1}$$

Modern configurations of the apparatus can also incorporate bender elements within the same set up allowing comparison between measurements made using the two methods. The resonant column can determine the dynamic properties of soils in the range of 0.001-0.1% (Hardin and Drnevich 1972; Richart, Hall, and Woods 1970) while bender elements measurements involve strains of <0.0001%.

Errors in resonant column test measurements typically result from a combination of several factors including e.g., sample disturbance, inhomogeneity of reformed samples, calibration errors and exceeding apparatus limitations.

A new Hardin-type fixed-partly fixed resonant column apparatus (RCA) with bender elements has recently been commissioned at the University of Glasgow. This paper describes the calibration procedure followed and investigates the limitations of the apparatus. The aim was to identify and reduce errors through rigorous calibration and procedural improvements, and to identify and quantify the contribution of apparatus limitations to errors in testing results.

2. Background

Several different designs of RCA exist, commonly categorised based on their different boundary conditions. The Hardin-type device used in this study and shown in Fig. 1 (GDS Instruments UK) is referred to in ASTM D4015 as 'device type 1' (ASTM 2021). A cylindrical soil sample enclosed in a latex membrane is mounted within a pressurised cell equivalent to a standard triaxial cell, with effective stress states achieved analogously. The lower end of the sample is rigidly attached to the base of the apparatus, (sometimes referred to as the 'passive end'), while the upper end is connected to a top cap. Porous disks are used at either end of the sample to allow drainage; these may be grooved or bladed to reduce slippage. The top cap is in turn connected to a drive plate which has four radial rotor arms with permanent magnets fixed at the ends. An accelerometer is mounted partway along one of the four arms, balanced by a counterweight on the opposing arm. This entire assembly consisting of
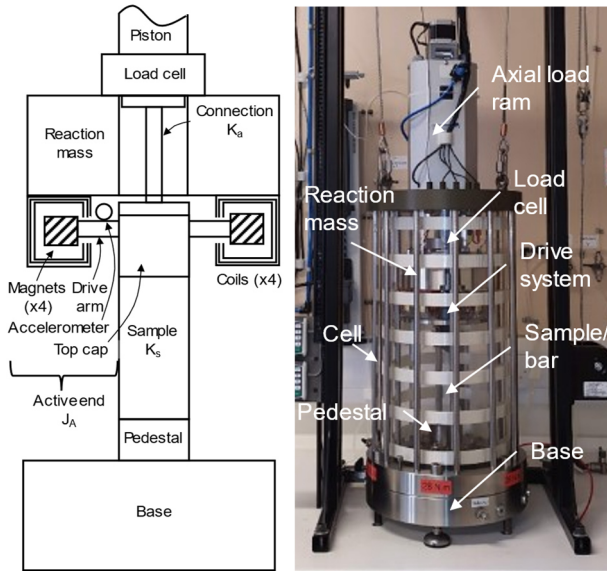
Figure 1. a) Schematic of the Hardin-type resonant column apparatus. b) Hardin-type resonant column apparatus (GDS Instruments UK) at the University of Glasgow.

the top cap, drive plate, accelerometer, counterweight, and magnets, plus any other attached components such as porous disks, screws and bolts, O-rings, etc. is referred to as the 'active end' and is assumed to behave as a single, rigid body. Each of the four magnet blocks sits within one of four drive coils, which are mounted to a large, steel reaction mass above the drive system. When a sinusoidal current is passed through these coils, a sinusoidal torque is generated in the permanent magnets which is transferred to the sample through the active end. The resulting torsional motion of the active end is detected by the accelerometer. The frequency of driving oscillations is varied until the first-mode resonant frequency, f_r, is found. If the sample is assumed to be isotropic, homogeneous, and to behave elastically in the range of torsional strains being applied, then the system may be treated as a one degree of freedom (1DOF) torsional pendulum. Solutions for this system (Richart, Hall, and Woods 1970) allow the shear wave velocity to be extracted for a measured value of f_r, which in turn is used to calculate G_0 for the sample.

The Hardin-type RCA shown above has the unique advantage of being able to test under anisotropic stress states. This is accomplished via an axial load ram whose piston passes through the top of the cell and connects to a load cell attached to the reaction mass, which measures the applied deviator force independently of cell pressure. The entire assembly consisting of the load cell, reaction mass, and active end system may be vertically actuated by the ram, allowing the system to accommodate samples of varying lengths. Samples may also be mounted and coupled at both ends with a split-mould still in place, minimising disturbance. Since the active end must be free to rotate, the connection between the load cell/reaction mass and the active end is accomplished via a slender, hollow aluminium shaft, which has high compressive stiffness but a relatively low torsional stiffness. The Hardin-type RCA is frequently described as having 'fixed - partly fixed' boundary conditions because the bottom of the sample is effectively held stationary by the base, while the top is free to rotate in torsion but is

constrained in flexion and extension by the drive connection. For these boundary conditions to hold, both the reaction mass and the base must be sufficiently massive to ensure that their motion during testing is negligible (Drnevich 1978a; ASTM 2021; Hardin and Music 1965).

Calibration of the RCA requires the rotational inertia of the active end, J_a, to be found. Rotational inertia is solely a product of mass and geometry and may be calculated directly. However, due to the complexity of the active end it is usually more convenient to determine J_a from a calibration exercise. This typically involves the use of one or more aluminium bars in place of a soil sample and may also include the use of attached masses. While J_a is by definition a constant, various studies (Clayton et al. 2009; Senetakis and He 2017; Shinde and Kumar 2021; Li, He, and Senetakis 2018) have reported an apparent variation in J_a with frequency when determined using these calibration methods.

An additional complication exists for Hardin-type devices, since the shaft which connects the load cell/ reaction mass to the active end has its own torsional stiffness, k_a, which behaves as an effectively massless torsional spring in parallel with the stiffness of the sample/calibration bar, k_s (B. O. Hardin and Music 1965). This gives an equivalent system stiffness, k_{eq}:

$$k_{eq} = k_a + k_s \qquad (2)$$

The calibration procedure for such devices must therefore also determine k_a so that its effects may be accounted for during tests on real soil specimens. Note that for 'fixed-free' devices, k_{eq} is simply equal to k_s.

If damping is low and the rotational inertia of the calibration bar is negligible compared to J_a then the equivalent system stiffness, k_{eq}, for a 1DOF torsional pendulum system of resonant frequency f_r is given by (Drnevich 1978a):

$$k_{eq} = (2\pi f_r)^2 J_a \qquad (3)$$

Note that the inertia of real soil specimens generally may not be neglected in this way, and a more rigorous approach is required (ASTM 2021).

3. Calibration

3.1. ASTM D4015 A2.1 Method

ASTM D4015 (ASTM 2021) outlines several methods for finding J_a. In all cases, the first step is to determine the apparatus resonant frequency, f_a, which is related to the apparatus stiffness, k_a, by:

$$k_a = (2\pi f_a)^2 J_a \qquad (4)$$

The standard recommends that this be accomplished by running a resonance test with the apparatus set up as it would be used during a test, but with no bar or sample present; f_a is the natural resonant frequency of the system in this configuration. For the device used in this study, f_a determined with this method was found to be 47.9 Hz.

To find the rotational inertia of the active end, J_a, the procedure given in ASTM D4015 A2.1 was used. One or more metal calibration bars of varying torsional stiffness, k_s, are fixed in place of a sample and the resonant

frequency of the system, f_r is determined. By combining Eqs. (2), (3) and (4), J_a is then given by

$$J_a = \frac{k_s}{(2\pi)^2[f_r^2 - f_a^2]} \qquad (5)$$

In this study a total of nine bars were tested. These were turned from solid billets of aluminium 6082, with lengths of either 100 mm or 140 mm, and nominal diameters ranging from 10 mm to 25 mm (see Fig. 2 and Table 1). Each bar was capped at both ends by a disc of 50 mm diameter and 5 mm thickness, which was used to secure the bar to the top cap and base pedestal with 3×4 mm Allen bolts. Aluminium was chosen because of its high shear modulus relative to its density, which allowed the rotational inertia of the calibration bars to be neglected (the rotational inertia of the thickest bar was found to be less than 0.5% the estimated active end inertia). Based on an assessment of reported values in the literature, the shear modulus, G_0, of aluminium 6082 was taken to be 26.0 GPa. The torsional stiffness of each bar is given by:

$$k_s = \frac{I_p G}{L} \qquad (6)$$

Where L is the length of the central portion of the bar (not including the end caps used for mounting which are assumed to be perfectly rigid) and I_p is the polar moment of inertia of a bar of diameter d, given by:

$$I_p = \frac{\pi d^4}{32} \qquad (7)$$

Because the calculated stiffness is strongly dependent on the diameter, it is recommended to obtain as accurate a measurement as practicable. In this study, a digital caliper was used to record diameter to the nearest 0.01mm at 20mm intervals along the length of the bar; these readings were then averaged. The average diameter of the bars was found to deviate from its nominal value by up to 2.4%, which would correspond to an error in calculated stiffness of 10.3%.

3.2. Added Masses Method

Equation (3) may be expressed in the form:

$$J_{am} = \frac{k_{eq}}{(2\pi f_r)^2} - J_a \qquad (8)$$

where J_{am} is the known rotational inertia of one or more masses rigidly attached to the active end during resonance testing. If a calibration bar is tested and the resonant frequency is found with several different attached masses, J_{am} may be plotted against $1/(2\pi f_r)^2$.

Figure 2. Calibration bars and masses used in the study.

Table 1. Dimensions of the central shaft of the calibration bars. Calculated stiffness neglects any end cap effects.

Bar	Length (mm)	Nominal diameter (mm)	Measured diameter (mm)	Calculated torsional stiffness (N·m/rad)
A1	140	10.0	9.85	172
A2	140	12.5	12.69	473
A3	140	15.0	14.74	861
A4	140	19.5	19.38	2574
A5	140	22.5	22.69	4834
A6	140	25.0	24.78	6873
B1	100	10.0	9.76	231
B2	100	12.5	12.70	664
B3	100	15.0	14.78	1216

If a straight line is fitted to these points, then by inspection of Eq. (8), the apparatus rotational inertia J_a is given by the negative intercept of this line on the y axis, and the equivalent system stiffness k_{eq} is given by the slope of the line (Clayton et al. 2009).

If the stiffness of the calibration bar, k_s, is found from Eqs. (6) and (7) then the apparatus stiffness, k_a, may be calculated from Eq. (2). If this process is repeated using several bars of varying stiffness, then each bar provides a measurement of both k_a and J_a. For Hardin-type devices, where the active end is supported by the ram assembly, measurements may also be taken using attached masses but with no bar or sample present.

This method vastly increases confidence in the value of k_a, which is otherwise obtained via a single measurement of resonant frequency with no bars or masses attached. In the case of devices such as the Stokoe-type RCA, which have no springs attached, this calibration method instead has the advantage that the bar stiffness, k_s, need not be known in order to obtain a measurement of J_a, since its value is not used in the determination of the intercept. This has the potential to reduce error compared to methods where the bar stiffness is used in calculations.

The added masses method was conducted for each of the bars detailed in Table 1, using annular stainless steel masses of 5.0 mm thickness with masses of 154.8 g, 227.8 g and 284.8 g, and rotational inertias of 0.000118 kg·m², 0.000241 kg·m² and 0.000365 kg·m² (see Fig. 2). For each bar the resonant frequency was recorded with each of the three masses attached, as well as with no masses attached. Only one mass was added at a time to minimise any effects of reduced coupling of the calibration bar end with the top cap by having multiple interfaces for slippage, and to avoid exceeding the fundamental assumption that the active end inertia is much smaller than the base/ reaction mass inertia.

3.3. Results and Discussion

Results from both calibration exercises are given in Fig. 3 and Table 2. The ASTM D4015 A2.1 method shows a weak increase in apparent J_a with frequency, dropping noticeably at frequencies approaching f_a. The substantial increase in apparent J_a observed by (Senetakis and He 2017) in the 130–170 Hz range (see Fig.3) was not repeated in this study; only modest increases at high

Table 2. Measurements of resonant frequency and torsional stiffness compared against their predicted values. A substantial over-prediction in resonant frequency is accompanied by a rise in the estimated dynamic torsional stiffness of the system.

Bar	Calculated torsional stiffness (N·m/rad)	Predicted resonant frequency (Hz)	Measured resonant frequency (Hz)	Measured system dynamic torsional stiffness (N·m/rad)	Estimated drive connection stiffness (N·m/rad)
None	0	48.8	47.9	481.6	481.6
A1	172	58.7	58.75	555.4	383.8
A2	473	72.9	71.9	864.2	391.7
A3	861	87.9	89.4	1297.5	436.4
A4	2574	135.5	133.6	2969.7	396.0
A5	4834	179.9	169.75	5299.6	465.5
A6	6873	212.2	200.5	10938.5	4065.7
B1	231	61.8	62.85	638.4	407.0
B2	664	80.6	79.1	969.6	305.6
B3	1216	99.6	100.45	1578.1	361.7

bar/sample stiffnesses were observed. This was unexpected because the results for the more flexible aluminium calibration bars were broadly similar to those for similar aluminum bars in that study and the apparatus was of very similar design. One possible explanation for this is the use of real soil samples by those Authors as calibration bars, with stiffnesses interpreted from bender elements which can be prone to errors. The added masses method shown on Fig. 3 and Fig. 4 shows comparatively little variation in apparent J_a for the range 58.75-133.6 Hz (bars A1-A4, B1-B3), with an average value in that range of 4.084×10^{-3} kg·m^2. The values of J_a and k_a obtained from the test with no bar present were noticeably elevated; k_a was 481.6 N·m/rad, whilst the average for bars A1-A4 and B1-B3 was 383.2 N·m/rad and remained relatively consistent in this range. By comparison, the stiffness of the connection bar as calculated from its design specifications is 370.3 N·m/rad, suggesting that the averaged k_a obtained by the added masses method is much closer to the true value. The behaviour of the apparatus when no bar or sample is present appears to deviate significantly from its behaviour with even the most flexible bar fitted. This may be explained as a lack of constraint in flexion of the top cap by a calibration bar; the resulting natural mode of vibration is not purely torsional but may also contain
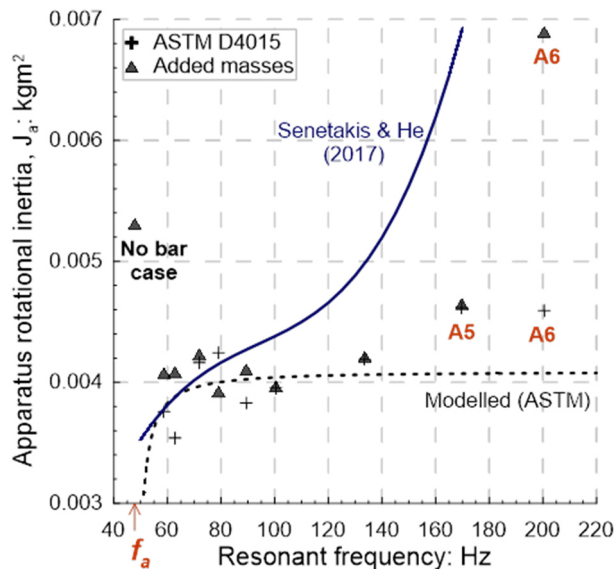
Figure 3. Apparatus rotational inertia versus resonant frequency determined using the ASTM D4015 A2.1 and added masses (Clayton et al., 2009) methods.

some flexural component which acts to lower the resonant frequency.

These results indicate that the method prescribed in ASTM D4015 of accounting for k_a by determining f_a may introduce large errors in estimates of J_a at resonant frequencies approaching f_a. This effect was investigated by assuming a constant k_a of 383 N·m/rad and J_a of 0.004084 kg·m^2, and back-calculating the output of Eq. (5) as a function of bar stiffness had the measured f_a of 47.9 Hz been used as in Section 3.1. This curve is plotted as a dashed line in Fig. 3 and explains why J_a appears to decrease as f_r approaches f_a, an effect also observed by (Senetakis and He 2017).

Results in the range 100 – 170 Hz are broadly similar for both methods, with a modest jump in estimated J_a seen for bar A5. In the added masses method, this was accompanied by a small increase in estimated k_a. For bar A6, the two methods diverge substantially. The ASTM D4015 A2.1 method shows no further increase in J_a while the added masses method shows a marked jump to 0.006895 kg·m^2, with an estimated k_a of 4066 N·m/rad, around 10 times higher than its average for the other bars. When the J_a value from the ASTM D4015 A2.1 method is used to compute the shear modulus, G_0, of bar A6, the output is within 1% of the known shear modulus of aluminium. By contrast, using the value of J_a from the added masses method results in a 54% over-estimation of G. This is clearly unacceptable and demonstrates that while the added masses method produces more consistent values of apparent Ja at lower stiffnesses than the ASTM D4015 A2.1 method, it should not be used to calibrate for high stiffness specimens. An explanation for the divergence between the two methods is given in Section 4.2.1.

Inspection of Fig. 4 illustrates how the error in the measured intercept increases substantially with the stiffness of the bar being tested, since the straight line being extrapolated from the data points becomes increasingly tangential to the y-axis.

3.4. Alternative Method

A third, alternative interpretation method was devised based on observations made in the previous subsection. Calculations of J_a using the measured resonant
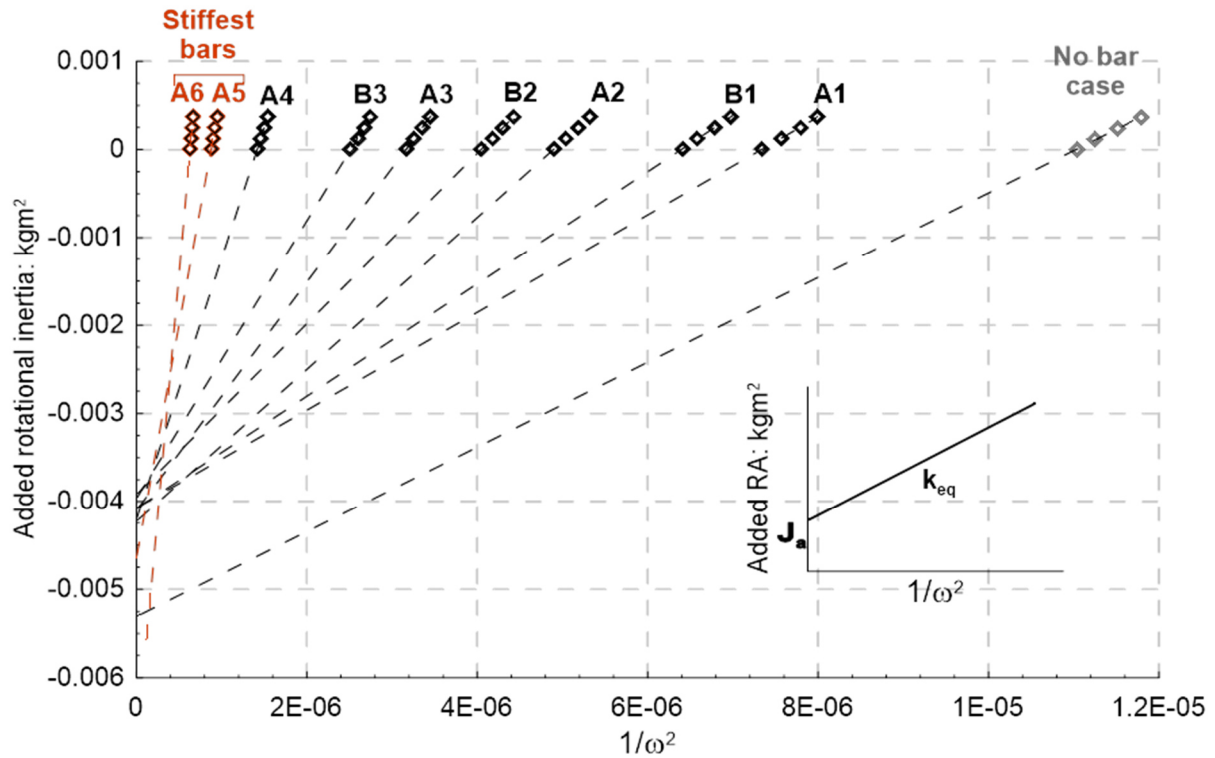
Figure 4. Method for finding Ja using bars and added masses (Clayton et al., 2009).

frequencies with no attached masses were made using the following expression derived from Eqs. (2) and (3):

$$J_a = \frac{k_s + k_a}{(2\pi f_r)^2} \tag{9}$$

This is analogous to the method in Section 3.1, except that the single measurement of f_a (shown to be susceptible to error) is replaced with the revised, averaged value of k_a of 383 N·m/rad from the added masses method. Results are presented in Fig. 5. This interpretation method gives the least variation in apparent J_a with resonant frequency of the three methods tested. Behaviour in the low- to medium-stiffness range is well-characterised by the constant, averaged values of J_a and k_a, while variation in apparent J_a at higher stiffnesses may
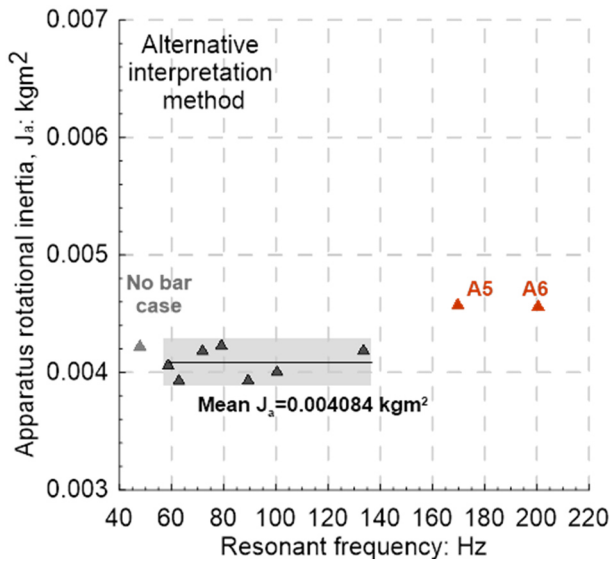

Figure 5. Alternative interpretation method showing range used to estimate Ja. This method shows the least variation in rotational inertia across the range of stiffnesses tested.

cautiously be accounted for by considering limiting conditions of the apparatus, as discussed in the following section.

4. Apparatus Limits

(Drnevich 1978b) recommends that for Hardin-type devices, the stiffness of the specimen should not exceed a limiting stiffness, k_L, of 3000 N·m/rad. This limit was based on devices available at the time. The corresponding limiting resonant frequency f_n is given by

$$f_n < f_a\sqrt{1 + k_L/k_a} \tag{10}$$

For the apparatus used in this study the limiting resonant frequency for k_L=3000 N·m/rad was calculated as 145 Hz, which coincides approximately with the point where the apparent J_a and k_a start to deviate. However, the observations made in Section 3.3 suggest that a more robust, apparatus-specific value of k_L could be obtained using the results of the calibration exercise.

(Clayton et al. 2009) identified a number of factors which may impact the measured resonant frequency at high stiffnesses. The most significant of these was that of drive system compliance, while the base inertia was also found to have some small effect. Their apparatus was of a 'fixed-free' design, where the drive reacts against a support frame rather than a reaction mass, so effects of reaction mass inertia were not investigated.

4.1. Effect of base and reaction mass inertia

To investigate the impact of the finite base and reaction mass inertias, the system was modelled as two different two degree of freedom (2DOF) torsional pendulum systems (shown in Fig. 6). In one, the base was considered perfectly fixed while the reaction mass was modelled as a second body of finite inertia. In the other,

the reaction mass was considered fixed while the base was modelled as a body of finite inertia. In both cases the active end was connected to the reaction mass by a massless spring of stiffness k_a and to the base by a massless spring of stiffness k_s (representing the drive connection and sample respectively, as defined previously). The reaction mass inertia and base inertia were estimated as 0.085 kg·m² and 0.56 kg·m² respectively from their known mass and approximate geometry. The natural modes of vibration for these systems were found and, in both cases, the favoured mode was clearly identifiable by its similarity to the 1DOF system mode. The change in frequency was compared to the 1DOF model. For the finite reaction mass model, the resonant frequency was observed to be most affected at low specimen stiffness, being 2.3% (1.2 Hz) higher at zero specimen stiffness, diminishing rapidly to 1.1% for bar A1 and falling below 0.1% for bars A4 - A6. For the finite base mass model, the resonant frequency was most affected at higher specimen stiffness but for the present apparatus the resonant frequency for the stiffest bar, A6, was only 0.3% (around 0.7 Hz) higher than that predicted by the 1DOF model

These results indicate that when testing soft materials in a Hardin-type device, the stiffness of the softest specimen to be tested should be no less than approximately 1/3rd the stiffness of the drive connection, in order to keep the error in resonant frequency below 1%. For the range of stiff bars tested in this study, neither the base inertia nor reaction mass inertia was found to significantly impact resonant frequency.

4.2. Effect of drive system compliance

(Clayton et al. 2009) identified compliance of the drive system as a significant contributor to error in measured resonant frequency. The 1DOF model explicitly assumes that the entire active end behaves as a single, perfectly rigid body of infinite stiffness. However, since the rotational inertia of the active end must be small compared to that of the base (and reaction mass), components must be kept fairly lightweight, suggesting that flexion of the relatively thin drive rotor arms may be

an issue. This issue is compounded because most of the mass of the active end is contained in the permanent magnets, which exist at the furthest point from the axis of rotation where their contribution to the rotational inertia is greatest. (Clayton et al. 2009) used finite element analysis to model the effects of the drive arm compliance for a bar of stiffness 9441 N·m/rad and observed a reduction in resonant frequency of around 10 Hz compared to the value predicted by the 1DOF system.

To investigate the effects of the drive system compliance in the present apparatus, the system was modelled as the 2DOF torsional pendulum shown in Fig. 7b, where the inertia of the inner portion of the active end, J_{a1}, represents one body and the permanent magnets represent a second body, J_{a2}, connected by a torsional spring of stiffness k_d representing the total stiffness of the drive system. Since most of the compliance is expected to be occurring in the four relatively thin drive rotor arms, which have very little mass themselves, this spring can be assumed to be massless. The first body representing the inner portion of the active end is connected to the parallel spring system formed by k_a and k_s with equivalent stiffness k_{eq}, which is fixed rigidly at its opposite end. (This condition assumes that the base inertia and reaction mass inertia are both sufficiently large that they may both be considered rigid bodies, which was validated in the previous subsection.)

The total rotational inertia of the permanent magnets was estimated to be 0.003538 kg·m² based on their known mass and the moment arm from their centre of mass to the axis of rotation. This represents approximately 87% of the total rotational inertia of the active end. Using the averaged values of J_a= 0.004084 kg·m² and k_a=383 N·m/rad from Section 3, predicted resonant frequencies for several different values of k_d were calculated and are plotted alongside the measured data in Fig 8.

Based on these results, the drop in observed resonant frequency corresponds to a drive stiffness of around 40,000 N·m/rad. At this value of k_d the predicted resonant frequency for bar A6 from the 2DOF model is 6.3% (13.3 Hz) lower than that predicted by the 1DOF model. This would correspond to an error of 13% in the calculated
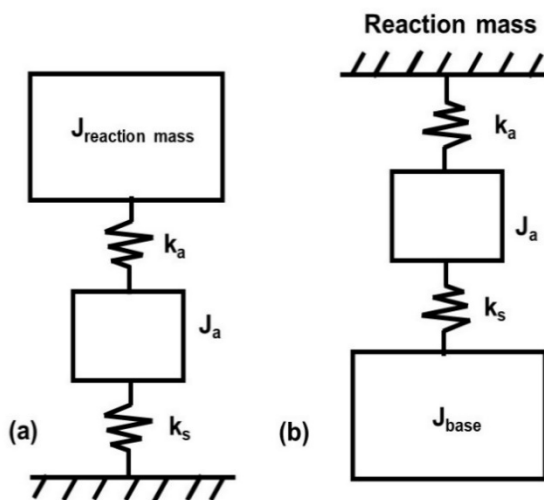
Figure 6. The effects of the a) reaction mass and b) base inertias were independently modelled as two degree-of-freedom torsional pendula.
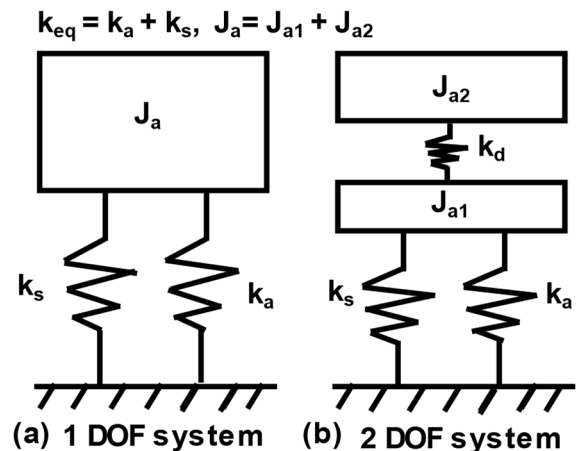
Figure 7. Comparison of (a) the standard one degree of freedom torsional pendulum model for Hardin-type resonant columns and (b) the two degree of freedom system used to model the effect of drive system compliance.
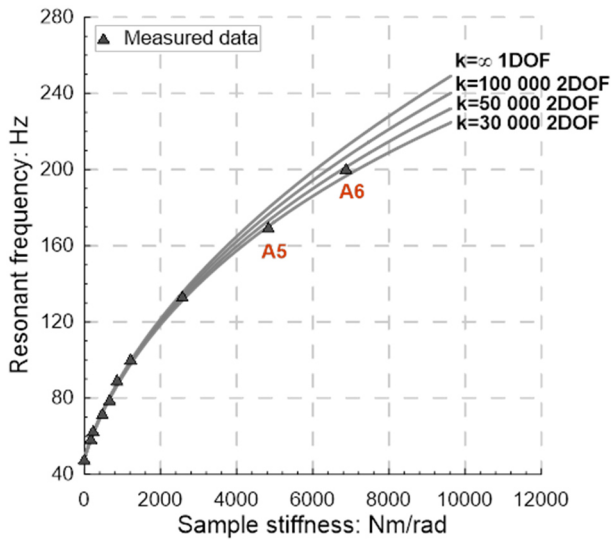
Figure 8. Effect of drive system compliance. This assumes that the stiffness of the calibration bars can be found from simple geometry.

shear modulus. It is difficult, however, to isolate the effect of drive stiffness from other potential influences on resonant frequency at high strains, such as slippage at the bar–top cap interface, and end cap effects of the calibration bars, all of which were found by (Clayton et al. 2009) to have some influence. Uncertainty is high due to scatter in the small number of data points, (2), used to determine k_d. Clearly more data at high stiffnesses are needed to accurately account for this effect.

4.2.1. Implications for the added masses method and for real soil specimens

From Eq. (4), f_r could be expected to reduce if the dynamic torsional stiffness, k_{eq}, was lowered by e.g., imperfect fixity of the calibration bar ends, failure to account for calibration bar end-cap stiffness, or stress-distribution effects (Clayton et al. 2009). In this case, inputting values of k_s which do not account for these effects would reduce the apparent k_a seen in the added masses method. However, these effects cannot explain the observed increase in k_{eq} compared to its expected value, accompanied by an increase in apparent J_a. This effect of both dynamic torsional stiffness and active end inertia appearing to increase dramatically was also observed by (Clayton et al. 2009) for a very stiff bar. Additionally, dynamic torsional stiffness was not seen to drop for any of the bars in that study, even as measured frequency reduced significantly from that predicted.

In the added masses method, masses are attached to the central portion of the active end. In the 2DOF model, this would correspond to J_{a1} becoming $J_{a1} + J_{am}$ while J_{a2} remains constant. Accounting for J_{am} in the model showed that the reduction in resonant frequency as a result of drive stiffness diminishes as $J_{a1} + J_{am}$ increases relative to J_{a2}; for bar A6 this reduction was 5.4% with the heaviest added mass compared to 6.3% with no added mass. This dependency on J_{am} has the effect of increasing the gradient of the straight line fit in Fig. 4, leading to an over-estimation of dynamic torsional stiffness, k_{eq}, and active end inertia, J_a, as seen in this study and in (Clayton et al. 2009). This explains why the ASTM D4015 A2.1

method and the added masses method diverge at high frequencies (the former uses no added masses, therefore this effect is not encountered). Since this effect occurs only when the assumption of active end rigidity fails, an apparent k_{eq} well in excess of its predicted value indicates significant drive flexion. If no further correction factors are to be used, then the frequency at which this effect first becomes significant may be considered a cut-off frequency for the apparatus. It may be possible to use a very stiff bar in combination with several added masses to observe the variation in the drive stiffness effect as the ratio of $J_{a1} + J_{am}$ to J_{a2} is varied, and thus derive a value for the drive stiffness, k_d. This would require that the effects of the base and reaction mass inertias either remain negligible or are properly accounted for.

When frequency correction factors, (1.045 and 1.063), derived from the 2DOF model using k_d=40,000 N·m/rad were applied to the measured resonant frequencies for bars A5 and A6 respectively, and the constant, averaged values of J_a= 0.004084 kg·m^2 and k_a=383 N·m/rad from Section 3 were used, the error in calculated shear modulus, G_0, for those bars reduced from 12% to 3% for bar A5 and from 11% to 1% for bar A6 compared to results using the uncorrected frequencies. This indicates that where other effects are properly accounted for, frequency correction factors derived from accurate estimation of drive stiffness could extend the useful range of resonant column devices beyond existing stiffness limits.

It is expected that testing with real soil samples with non-negligible rotational inertia (particularly larger diameter samples) would similarly influence the drive stiffness error, since the top of the sample is considered as being fixed to the top cap and rotates with the active end. Therefore, when switching between sample sizes or when testing samples of substantially different densities, any frequency correction factors used to extend the upper limit of sample stiffness should be modified to account for sample inertia. This should reduce errors when testing stiff soil samples, since previous calibration methods relying on an inconstant J_a derived from effectively massless calibration bars do not account for differences in the drive stiffness effect for soil samples having significant inertia.

5. Conclusions

This paper has described different approaches to calibrate a Hardin-type fixed-partly fixed resonant column apparatus. The following conclusions are drawn from the work:
  a) Calibration of the resonant column requires accurate determination of the rotational inertia of the active end, J_a, which is found using a calibration exercise involving either bars of known stiffness or bars of known stiffness and added masses of known rotational inertia;
  b) The ASTM D4015 A2.1 method and the added masses method were considered. The obtained value of J_a and its apparent variation with frequency was shown to be highly dependent on the calibration method. Both methods showed substantial variation in apparent J_a within the range

of stiffnesses tested, although this variation was less than reported elsewhere in the literature.

c) When using any calibration method where the bar stiffness is used in calculations, it is important to determine the diameter of the bar(s) to a high level of accuracy.

d) For Hardin-type devices, the method of compensating for the drive connection stiffness by finding the apparatus resonant frequency, f_a with no bar or sample was found to be prone to error. Errors in this value are most impactful when testing very soft materials, and in this case it is advisable to determine the drive connection stiffness using the added masses method with several different flexible bars and average the results.

e) The added masses method reduces scatter in J_a for more flexible calibration bars but is susceptible to error at high stiffnesses.

f) An alternative interpretation approach is suggested here which combines the two calibration methods tested. This approach gives the least variation in apparent active end inertia. Below the limiting stiffness of the apparatus, J_a may be assumed to be constant in calculations of G_o with no further adjustments needed.

g) An unexplained increase in apparent J_a, (and/ or apparent dynamic torsional stiffnesss, as found with the added masses method), with increasing calibration bar stiffness is a strong indication that the apparatus limits have been exceeded and may be used to derive a sensible limiting stiffness for the apparatus.

h) The base inertia and reaction mass inertia are not found to significantly impact resonant frequency for the apparatus used in this study, except for very soft samples or for samples exceeding the range of stiffnesses tested.

i) The compliance of the drive system contributes significantly to the reduction of resonant frequency for stiff samples. This reduction in resonant frequency may be modelled with some accuracy and used to derive frequency correction factors. When these frequency correction factors are used to modify the measured resonant frequencies, the active end rotational inertia can be treated as constant over the full range of calibration stiffnesses. Additional calibration in the high stiffness range should increase confidence in these correction factors and allow the upper limit of stiffness for the device to be further increased.

j) Since the frequency reduction effect of the drive system compliance is likely to be dependent on sample inertia, calibration methods which do not account for the substantial difference in inertia between calibration bars and real soil specimens may introduce errors at high stiffnesses. The use of frequency correction factors, which may be readily adjusted to account for different specimen inertias, may reduce this error.

k) Since the impact of drive system compliance was several times greater than that of the base inertia at high resonant frequencies, a second, stiffened drive plate could be used to reduce drive arm flexion when testing very stiff specimens. The additional weight penalty should be more than compensated for by the reduction in drive system compliance.

Acknowledgements

References

ASTM. 2021. "Standard Test Methods for Modulus and Damping of Soils by Fixed-Base Resonant Column Devices 1." https://doi.org/10.1520/D4015-21

Clayton, C. R.I., J. A. Priest, M. Bui, A. Zervos, and S. G. Kim. 2009. "The Stokoe Resonant Column Apparatus: Effects of Stiffness, Mass and Specimen Fixity." Geotechnique 59 (5): 429–37. https://doi.org/10.1680/geot.2007.00096

Drnevich, V. P. 1978a. "Modulus and Damping of Soils by the Resonant-Column Method." Dynamic Geotechnical Testing.

Drnevich, V. P. 1978b. "Resonant-Column Testing Problems and Solutions." Dynamic Geotechnical Testing.

Hardin, B. O., and J. Music. 1965. "Apparatus for Vibration of Soil Specimens During the Triaxial Test." Instruments and Apparatus for Soil and Rock Mechanics, September, 55-55–20. https://doi.org/10.1520/STP41278S

Hardin, B. O., and V. P. Drnevich. 1972. "Shear Modulus and Damping in Soils: Design Equations and Curves." Journal of the Soil Mechanics and Foundations Division 98 (7): 667–92. https://doi.org/10.1061/JSFEAQ.0001760

Li, H., H. He, and K. Senetakis. 2018. "Calibration Exercise of a Hardin-Type Resonant Column." Geotechnique 68 (2): 171–76. https://doi.org/10.1680/jgeot.16.P.214

Richart, F. E, J. R. Hall, and R. D. Woods. 1970. Vibrations of Soils and Foundations.

Senetakis, K., and H. He. 2017. "Dynamic Characterization of a Biogenic Sand with a Resonant Column of Fixed-Partly Fixed Boundary Conditions." Soil Dynamics and Earthquake Engineering 95 (April): 180–87. https://doi.org/10.1016/j.soildyn.2017.01.042

Shinde, N. S., and J. Kumar. 2021. "Calibration Exercise of Fixed-Free Resonant Column Apparatus." In Lecture Notes in Civil Engineering, 119 LNCE:35–42. Springer Science and Business Media Deutschland GmbH. https://doi.org/10.1007/978-981-33-4001-5_4